Probing the magnetic field dependence of the light hole transition in GaAs/AlGaAs quantum wells using optically pumped NMR

Matthew M. Willmering, Erika L. Sesti, Sophia E. Hayes, Ryan M. Wood, Clifford R. Bowers, Sunil K. Thapa, Christopher J. Stanton, Arneil P. Reyes, Philip Kuhns, and Stephen McGill

Phys. Rev. B **97**, 075303 — Published 7 February 2018

DOI: 10.1103/PhysRevB.97.075303

preprintAPS/123-QED

Probing the magnetic field dependence of the light hole transition in GaAs/AlGaAs quantum wells using optically pumped NMR

Matthew M. Willmering, Erika L. Sesti, and Sophia E. Hayes*
Chemistry Department, Washington University in St. Louis, 1 Brookings Drive, St. Louis, Missouri 63130, USA

Ryan M. Wood and Clifford R. Bowers
Chemistry Department, University of Florida, Gainesville, Florida 32611, USA

Sunil K. Thapa and Christopher J. Stanton*
Physics Department, University of Florida, Gainesville, Florida 32611, USA

Arneil P. Reyes, Philip Kuhns, and Stephen McGill
National High Magnetic Field Lab, 1800 E. Paul Dirac Drive, Tallahassee, Florida 32310, USA
(Dated: January 16, 2018)

Optically pumped NMR (OPNMR) of the NMR-active $^{69/71}$Ga species has been shown to be a unique method to probe electronic energy bands in GaAs, with sensitivity to the light hole-to-conduction band transition. This transition is often obscured in other optical measurements such as magneto-absorption. Using OPNMR, we exploit the hyperfine interaction between conduction band electrons (and their spin states) and nuclear spins, which are detected through phase-sensitive radio-frequency (NMR) spectroscopy. Measurements were made over a range of external magnetic fields (B_0) in two different labs with separate experimental setups to obtain the magnetic field dependence of the light-hole-to-conduction band transition energy. In addition, $k \cdot p$ theory was used to interpret the experimental results, mapping out this specific transition's magnetic field dependence in an AlGaAs/GaAs quantum well. The combination of theory and experiment point to a mixing of valence bands at a field of approximately $B_0 = 4.7$ T, swapping the dominant character of the absorption transition and, thus, explaining the magnetic field dependence. Lastly, the experimental dependence of the light-hole-to-conduction band transition energy on B_0 is found to be less steep compared to the calculated trend, indicating that inclusion of additional effects may be necessary to accurately model the spin-split band structure. The additional insight gained by $^{69/71}$Ga OPNMR about the light hole states will facilitate future testing of more complex band structure models.

I. INTRODUCTION

Semiconductor energy band diagrams provide information which is useful for determining how a semiconductor will behave in electronic devices. While conventional optical spectroscopy can effectively probe the states near the band edge (energy states at the maximum of the valence band (VB) and minimum of the conduction band (CB)), techniques to probe the deeper bands are lacking. Thus, in order to fully understand and improve the theory of band diagrams, one must develop experimental methods to observe the deeper bands to facilitate comparisons with theoretical calculations.

For GaAs, a zincblende semiconductor, the valence band has three energy bands: light hole (LH), heavy hole (HH), and split-off hole (SH). The LH and HH bands are degenerate at $k = 0$. Optical transitions from these states can be exploited in OPNMR (optically pumped nuclear magnetic resonance) to polarize the electron spins and ultimately the nuclear spins via the Fermi contact hyperfine interaction[1]. OPNMR is typically performed in semiconductors at temperatures < 10 K where the phonon-mediated nuclear spin relaxation is quenched, allowing the electron-nuclear flip-flop term of the hyperfine interaction to be dominate, resulting in hyperpolarized nuclear polarization. This increased nuclear spin polarization boosts the sensitivity of NMR experiments, which reduces the number of NMR active nuclei required to observe a signal. OPNMR experiments can be performed as a function of photon energy, resulting in an OPNMR "profile"[2–6]. While other factors, such as penetration depth[7,8], can affect the total nuclear polarization, resolved spin oriented transitions can be seen as peaks and valleys in the OPNMR profile. The OPNMR profile depends on the magnetic field-split band structure of the semiconductor and the transition intensities, allowing one to identify features in the band structure such as Landau levels (LLs)[2,3,9–11]. Recently, it has been shown that OPNMR can also be used to observe the interband LH transition which is deeper in the valence band[10–12]. Thus, OPNMR is a suitable technique for probing deeper valence energy bands and their mixing.

Since spin oriented electrons lead to the enhanced nuclear spin polarization, it is important to understand the processes underlying OPNMR that lead to electron spin polarization. When illuminating with circularly polarized light (σ^+ or σ^-), each photon carries with it either +1 or -1 unit of angular momentum, respectively, which

gives rise to interband transitions that conserve both energy and total angular momentum[13]. In sufficiently narrow quantum wells (studied in this experiment), confinement in the z direction induces an energy separation for the HH and LH bands at $k = 0$. Therefore, a higher photon energy is required to excite from the LH band to the bottom of the CB than from the HH band, shown schematically in Fig. 1.

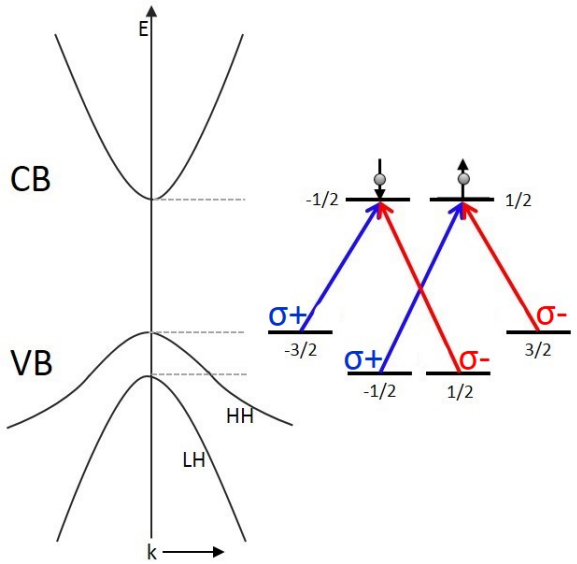

FIG. 1. Conduction (CB) and valence band (VB) schematic showing the transitions from the heavy (HH) and light hole (LH) bands to the bottom of the conduction band using circularly polarized light. The LH and HH bands are split at $k = 0$ due to the quantum confinement effects present in quantum wells. Allowed σ^+ light transitions are represented by blue arrows while σ^- is represented by red arrows.

As shown in Fig. 1, the transitions from the VB are determined by the polarization of the light. The resulting electron spin polarization, when excited from the LH band, is opposite to that of the HH band, for the same helicity of the circularly polarized light. When a magnetic field is applied, the bands form subband LLs which can be detected with OPNMR[10,14]. Allowed interband transitions are now not only limited by conservation of total angular momentum ($\Delta m_j = \pm 1$) but also by the change in the subband LL quantum number. The focus of our measurements is to implement OPNMR in order to measure the LH-to-CB transition, as a function of the applied magnetic field. Polarized photoluminescence excitation (PLE) spectroscopy was also performed to complement the OPNMR measurements which were performed in two different laboratories. OPNMR data with external magnetic fields (B_0) in the 4 T – 11.8 T range were acquired at the National High Magnetic Field Laboratory (NHMFL) and additional data at 3 T and 4.7 T were obtained at Washington University (WUSTL). This facilitated the magnetic field dependence of LH-to-CB transition and band mixing effects to be investigated as a function of magnetic field.

II. EXPERIMENTAL

OPNMR experiments were performed at both the National High Magnetic Field Lab (Tallahassee, FL) and Washington University. Polarized photoluminescence excitation (PLE) was performed at Washington University as well. The sample was grown on a single crystal bulk GaAs base substrate using the molecular beam epitaxy (MBE) method at the Ruhr Universität in Bochum, Germany. The sample contained multiple (60) GaAs quantum wells separated by $Al_{0.31}Ga_{0.69}As$ (AlGaAs hereafter) barriers. The GaAs quantum wells were 16.9 nm thick with 24.5 nm barriers. The set of 60 quantum wells and barriers were sandwiched between superlattices. The sample was topped by a 10 nm GaAs capping layer. The total sample, including the substrate, was approximately 1 mm thick.

At both locations, the sample was mounted to a piece of sapphire to act as a heat sink, using Apiezon grease. Temperature was monitored using a Lakeshore 340 temperature controller, and homebuilt single-channel NMR probes were used to acquire the NMR data. The probe and sample were inserted into a space which was evacuated then back-filled with a small amount of He gas. In both experimental setups, the plane of the quantum well was perpendicular to the magnetic field, which is parallel to the laser propagation direction.

A. OPNMR at NHMFL

The NHMFL OPNMR experiments employed a vertical variable superconducting magnet that can reach up to 17.5 Tesla. The magnet has a sealed cold bore which provides the cooling to hold the sample space at 4.5 ± 0.5 K. ^{71}Ga NMR was obtained at low magnetic fields while ^{69}Ga NMR was obtained for the highest field due to the tuning frequency range of the probe[15]. The NMR spectra were recorded on a homebuilt spectrometer using a PTS 3200 frequency synthesizer and a CPC MRI Plus amplifier. The number of transients recorded for each spectrum was four, using phase cycling.

A Coherent Verdi laser (at 5 W) was used to pump a Coherent Ti:Sapphire Mira 900 laser with an approximate linewidth of 0.4 meV at these wavelengths. The beam was focused to have an approximate 3 mm spot size at the sample. The wavelength of the laser was monitored using a 0.75 m McPherson monochromator with a 600 grooves/mm grating and a charge-coupled device (CCD) camera. The laser power was held at 200 mW (2.8 W/cm^2) and was measured before entering the bore of the magnet. The power was measured using an Ophir Nova Power Meter. A quarterwave retarder was used to

create circularly polarized light. The sample was irradiated for 30 seconds (τ_L) for each scan.

B. OPNMR and Polarized PLE at WUSTL

The WUSTL lab employed two horizontal superconducting magnets with magnetic fields of 3.0 T and 4.7 T. A helium recirculating cryostat made by Janis (SHI 950) is used to keep the sample at 6 ± 0.3 K. The NMR spectra were recorded on a Tecmag Apollo spectrometer. A single transient was acquired at each wavelength used for optical pumping. ^{69}Ga NMR was obtained for all points.

A Spectra Physics Millenia X laser (at 10 W) was used to pump a Coherent Ti:Sapphire 899-21 ring laser with an approximate linewidth of 30 MHz. The beam was focused to have an approximate 2 mm spot size at the sample. The sample was irradiated for 60 seconds (τ_L). The wavelength of the laser was monitored using a Bristol 521 Wavelength Meter which has a 0.01 nm resolution. The laser power was held at 100 mW (3.2 W/cm^2) for the 4.7 T profile and 200 mW (6.4 W/cm^2) for the 3 T profile. The power was measured before the magnet bore using a Coherent FieldMate Power Meter. The laser passed through a quarterwave retarder in order to create circularly polarized light.

Polarized photoluminescence was collected after passing through a photoelastic modulator (PEM) (Hinds Instruments PEM-100) and a beam splitter cube before reaching the monochromator (Acton SpectraPro-2750; 0.75m path length) and being detected by an avalanche photodiode (APD) detector. A lock-in amplifier (Stanford Instruments SR-830) and a low-pass filter (Stanford Instruments SR-640) were used to lock on to the PEM frequency and measure the total light emission, respectively.

C. OPNMR Procedure

The populations of the nuclear spin states of the gallium isotope being measured by NMR was first saturated using a standard saturation pulse sequence to destroy any magnetization that has built up between experiments (due to relaxation processes). Thus, the recycle delay (1 s) is inconsequential since the initial magnetization is destroyed at the start of the experiment. The pulse sequence can be seen in Fig. 2. Saturation was followed by a period of time (τ_L) where the polarized laser pumped the sample. τ_L here is defined as the time between the saturation train and the Bloch decay sequence for detection. Even though the two locations (WUSTL and NHMFL) used a different τ_L time and power density, no effect on the transition energy measurement is expected. A longer pumping time generally results in more signal. More signal (i.e. greater S/N of the NMR spectra) results in smaller error bars for the points in the OPNMR profile and should have no effect on the energy levels of the bands. A higher power density increases the number of polarized electrons in the CB which can increase the polarization rate (i.e. decrease the length of τ_L irradiation time needed to achieve a certain S/N). Both locations used power densities low enough to avoid sample heating and electron-electron correlation effects which could affect the energy levels. A $\frac{\pi}{2}$ radio frequency (rf) pulse (6±1 μs with both setups at all fields) was applied prior to acquisition. The probes were tuned at each external field, and comparable impedance matches were obtained. This allowed for similar B_1 strengths (only dependent on the rf amplifiers frequency dependency gain curve) and thus a consistent pulse length can be used without sacrificing signal. The $\frac{\pi}{2}$ pulse length was optimized under optical pumping conditions at the photon energy which provided the largest signal intensity. The optical pumping conditions polarized the nuclei to a detectable limit. The standard $\frac{\pi}{2}$ rf pulse calibration was completed following the optical pumping for each pulse length acquisition.

FIG. 2. Pulse sequence used to obtain OPNMR data. The top rf portion shows a train of saturation pulses followed by a delay (τ_L) before the inspection pulse and acquisition. The bottom laser portion shows the laser is pumping the sample during the τ_L time period, the inspection pulse, and acquisition.

A thermally relaxed NMR spectrum was first acquired with an inspection pulse after allowing the nuclear T_1 process to occur for a given amount of time (typically overnight). No laser was used to optically pump the sample in order to obtain the Boltzmann thermally polarized spectrum. This spectrum is phased (conventionally) to be absorptive. The phase angle used for each OPNMR spectrum was the same phase used to make the thermal signal purely absorptive at each OPNMR setup. Each ^{69}Ga and ^{71}Ga spectrum was then fit with a Gaussian line shape in order to find the area of the peak. We choose to use areas of a fitted function rather than peak intensity to account for any fluctuations in linewidth. The areas of the NMR signals were then plotted as a function of photon energy in an OPNMR profile (Fig. 3).

The most apparent peak in the OPNMR profile attributed to the light hole transition[10,12] was then fit to a Gaussian as a guide to the eye (see Fig. 3) in order to extract the energy of the peak maximum for this feature as a function of photon energy. Lorentzian and Gaussian fits produce similar results and trends. However, Gaussian line shapes fit the data better.

D. Polarized PLE Procedure

Photoluminescence from the sample was directed through a PEM (at 50 kHz) and a beam splitter cube. The PEM transformed the circularly polarized light to into either vertically or horizontally polarized light depending on the helicity of the luminescence. In our set-up, only the horizontally polarized light is allowed to pass through the beam splitter cube into the monochromator. The PEM switches between converting the σ^+ and σ^- photoluminescence as horizontally polarized light. The lock-in amplifier locks in on the PEM frequency of 50 kHz and measures the difference between the intensities of σ^+ and σ^- photoluminescence. The difference can be normalized by the total photoluminescence measured by the low pass filter, resulting in the extrapolation of percent polarization of the luminescence.

For detecting the PLE, the monochromator was positioned to the low energy side (longer wavelength) of the luminescence feature (i.e., observe the HH). The signal was averaged for 10 s at multiple excitation energies in order to map out the LH transition. Similar to the OPNMR data, the inverted peak which crosses through zero polarization is fit with a Gaussian line shape in order to determine the peak maximum. These measurements were confined to lower and zero magnetic field strengths

E. THEORY AND CALCULATIONS

We have used empirical $k \cdot p$ theory based on the 8-band Pidgeon-Brown model for the calculation of energy band structure with nonzero magnetic field as well as the absorption coefficient. Additional details are contained in previous publications[11,12]. We use Pidgeon-Brown (PB) manifolds, $(p = -1, 0, 1, 2, ...)$, to label the energy bands and LL indices, $(n = 0, 1, 2, ...)$, for avoiding ambiguity in the transition selection rule. The LL for the different spin components of the envelope function are shown as left superscripts in Table I. For instance, in the $p = 2$, Pidgeon-Brown manifold, the first component is in a CB spin-up state in the $n = 1$ LL, the second component is in a HH spin up state in the $n = 0$ LL, etc.

Landau level index for each component in a PB manifold
$^{n=p-1}$CB$\uparrow$
$^{n=p-2}$HH$\uparrow$
$^{n=p}$LH$\downarrow$
$^{n=p}$SH$\downarrow$
$^{n=p}$CB$\downarrow$
$^{n=p+1}$HH$\downarrow$
$^{n=p-1}$LH$\uparrow$
$^{n=p-1}$SH$\uparrow$

TABLE I. Landau-level indicies (n) and basis states for the spin states in a given Pidgeon-Brown (PB) manifold = p.

Since the LL index must be ≥ 0, there is only 1, 4, 7 non-zero components to the envelope function for the PB manifolds = -1, 0, 1 respectively. For PB manifolds > 2, there are 8 components in each manifold. Thus, the PB manifolds will begin at $p = -1$ and increment by $+1$ for the inclusion of larger LL indices.

III. RESULTS AND DISCUSSION

OPNMR profiles were obtained for a region of photon energies around the expected LH transition. The resulting OPNMR profiles notably have resonances with both positive and negative peak amplitudes and concomitant areas. NMR signals for σ^- were found to be largely positive ("absorptively phased" spectra) except for the region in which the LH transition appears. Similarly, all of the σ^+ NMR signals were negative ("emissively phased" peaks) except where the transition occurs. The OPNMR profiles from the NHMFL measurements at various fields (4 T – 11.8 T) and the fits to the LH transition can be seen in Fig. 3.

In our earlier publications[10–12], we reported on the inversion in the sign of nuclear magnetization when optically pumping at the LH-to-CB transition. Through modeling[10,11], this assignment was confirmed for $B_0 =$ 4.7 T. We have sought to extend our experiments to additional B_0 fields in an effort to examine the B_0 dependence of this interband transition. The OPNMR profiles extracted from data recorded at NHMFL are depicted for external magnetic fields (B_0) of 4 T – 11.8 T. Fig. 3a shows these OPNMR profiles with σ^- laser irradiation, and Fig. 3b are those with σ^+ irradiation. Superimposed onto each are Gaussian functions fit to the peak where signal inversion occurs, meant to guide the eye. As expected, the LH transition shifts to higher photon energies as B_0 is increased, for both helicities of light. For σ^- irradiation at the LH transition, the magnetization of the OPNMR resonance becomes inverted (or much closer to zero for lower fields), exhibiting negative magnetization. For σ^+, the opposite is true: once the LH transition is irradiated, the signals adopt the opposite phase, such that the signals exhibit positive magnetization.

In Fig. 3, the transition appears much stronger and thus inverts the nuclei to a greater degree at higher fields. While not quantitative, this trend is notable since higher fields increase the splitting between the energy levels. The combination of quantum confinement (to separate the LH and HH bands) and higher magnetic field could be reducing the amount of HH character in the LH band due to band mixing. The same trend has been observed in the published Washington University data[10,12].

A. Field Dependence

Using the peak position of the transition attributed to the LH-to-CB, a plot of that transition energy versus external magnetic field has been constructed, shown

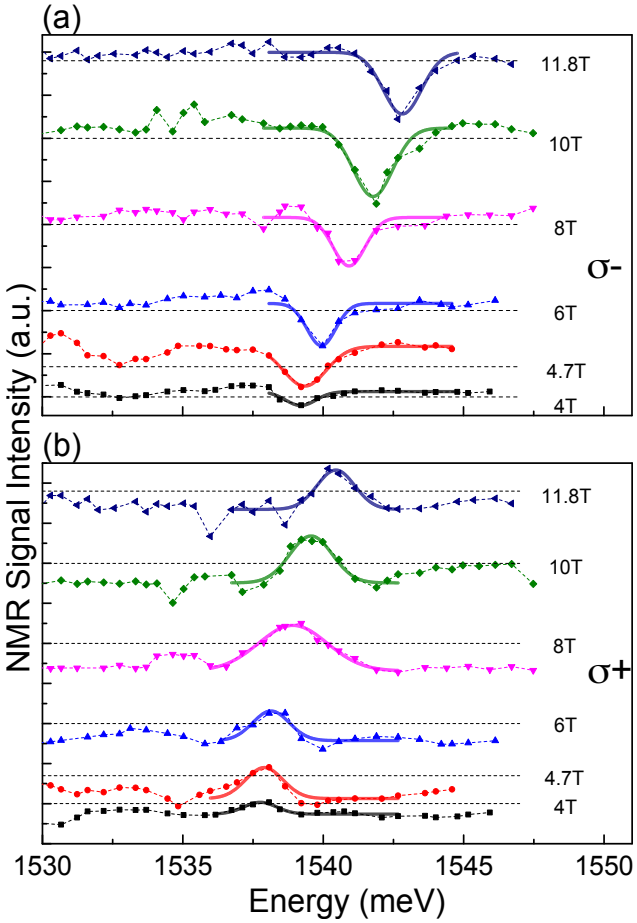

FIG. 3. ^{71}Ga and ^{69}Ga OPNMR profiles of AlGaAs/GaAs quantum wells at the magnetic fields indicated in the legend (4 T – 11.8 T) for a) σ^- laser irradiation and b) σ^+ laser irradiation. All profiles were taken at NHMFL. Profiles are offset for clarity. The black dashed line on each plot represents zero NMR signal. The Gaussian peaks, which are fits to the experimental data, (shown as solid curves) superimposed on the data in each plot are meant to guide the eye.

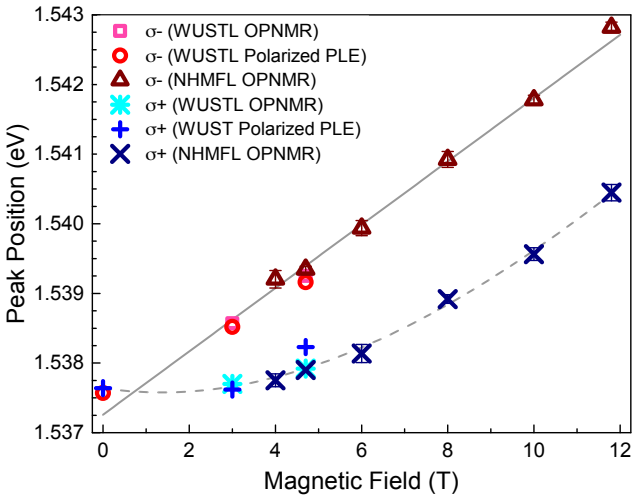

FIG. 4. Light hole-to-conduction band transition energies for σ^+ (blue crosses) and σ^- (red symbols) polarized light as a function of external magnetic field. Dark ✕'s and △'s represent OPNMR data taken at the NHMFL, light ✳'s and □'s represent OPNMR data from WUSTL, and medium +'s and ◯'s represent PLE data acquired at WUSTL. A solid linear least squares fit for σ^- data and a dashed cubic B-spline for the σ^+ data are shown as guides to the eye. Overlapping 4.7 T OPNMR data at both locations are shown and demonstrate the consistency of the measurement even with different set-ups.

in Fig. 4. We include data from both WUSTL (OPNMR and PLE) and NHMFL (OPNMR), as indicated in the legend. Notably, data were collected at 4.7 T at both labs, and the OPNMR data show excellent agreement in the LH transition energy, which lends confidence that small differences between equipment types and the resulting measurement have not affected the physical interpretation of the data. Also, both OPNMR and PLE data were acquired at 3 and 4.7 T at WUSTL. The 3 T PLE and OPNMR data match very well, showing both measurements of electron spin and nuclear spin polarization arising from the LH transition energy lead to the same conclusion. The 4.7 T PLE S/N is much smaller, introducing more error in the determination of the peak maximum.

Due to the large slope of the CB LLs with respect to the magnetic field, only the lowest-lying CB will be excited to for the energies studied here. Circularly polarized light will only excite transitions from specific valence band LL subbands to the lowest-lying CB LL. For the LH-to-CB transition, σ^- light would originate from the $p = 1$ hole LL (creating a spin down conduction electron) while the σ^+ light would originate from the $p = 0$ hole LL (creating a spin up conduction electron) in the Faraday geometry[16]. Consequently, the σ^+ and σ^- transitions will occur at different energies due to dissimilar initial states. The σ^+ and σ^- transitions are also split by the Zeeman interaction in proportion to the applied magnetic field. Importantly, each transition will also exhibit a dissimilar dependence on magnetic field, due to band mixing effects, as explained below.

σ^- irradiation reveals an approximate linear dependence of the LH transition with respect to the external magnetic field. Such a linear dependence has been observed for high magnetic fields[17,18], and similar linear trends have been observed before in reports of calculated and experimental measurements of absorption and photoluminescence data using circularly polarized light[16,19,20]. Similarly, transitions excited with σ^+ irradiation also show a linear dependence at high external magnetic fields (B_0= 6 to 12 T), but the slope decreases as the magnetic field decreases to zero.

Spin splitting of the CB and LH states is expected. For the CB, the subband LLs are linear with field, which

would not induce any curvature in the field dependence of the transition energy, as it appears in Fig. 4. In contrast, the valence subband levels do possess curvature. Similar results for field-dependent LL transitions have been modeled by Broido and Sham[17] and have shown curvature as a function of magnetic field where the onset and sharpness of the curvature depends on the LL of the electron and its spin orientation in the magnetic field. Since we are looking at the transition from the VB LH state to the CB state, we have to take into consideration how the magnetic field affects both bands in order to know the transition energy.

Furthermore, circularly polarized light can only excite from specific VB LLs to the lowest lying CB LL, depending on the helicity of the polarized light and selection rules, as shown below[16]. Since our final state is at the bottom of the CB, the allowed LH transitions for σ^- and σ^+ light must originate from different LLs, causing each transition to now have a dissimilar dependence on the magnetic field.

B. Simulation Results

To explain and interpret the OPNMR profile, we have calculated the electronic energy band structure, wavefunctions, optical absorption, and CB spin polarization. Our calculations are based on our previous works[10–12] where they are described in detail.

In Fig. 5, we have plotted the highest lying valence band Landau levels. Because GaAs is a relatively large gap semiconductor, there is little valence/conduction band mixing in the CBs. As a result, the CBs follow an approximate formula $E_n = (n + 1/2)\,\hbar\,(eB_0/m_e^* c)$. The Zeeman splitting for the CBs is weak (less than 0.5 meV at 10 T) and is not resolved in the OPNMR profiles.

Our valence subband LLs look similar to other calculations on slightly different structures[21,22]. Highlighted in the figure are the valence bands which give rise to the lowest LLs for the LH spin-up and LH spin-down. We label the bands as V_{ij}, where i is the Pidgeon-Brown manifold number and j labels the valence band states within the manifold. For example, V_{01} corresponds to the highest energy valence band states in the $p = 0$ Pidgeon-Brown manifold. The $p = 0$ states are in blue, while the $p = 1$ states are in red.

Looking at Table I, we see that the $n = 0$ LH spin-down LL ^{0}LH$\downarrow$ lies within the $p = 0$ Pidgeon-Brown manifold while the $n = 0$ LH spin-up ^{0}LH$\uparrow$ lies within the $p = 1$ Pidgeon-Brown manifold.

From Fig. 5, we note the following: 1) the LH bands lie *deep within the valence* subbands (and not near the top of the valence bands); 2) there is strong mixing within the valence bands.

The mixing of the valence band Landau levels can be quantified. This is shown for the $p = 0$ manifold in Table II. The V_{02} state is primarily the ^{0}LH$\downarrow$ state with a small mixture of the ^{1}HH$\downarrow$ at low B_0 fields. The tabulated probabilities indicate that for $p = 0$, the dominant valence band states are ^{1}HH$\downarrow$ and ^{0}LH$\downarrow$. We can see the swapping of probabilities between V_{01} and V_{02} at 4.7 T and beyond both in Table II (in blue) and graphically in Fig. 5 so that the replacement of V_{02} by V_{01} as the initial state in the optical transition occurs as the magnetic field is increased. For the most part, there is no hybridization between these two levels. As a result, we relabel the states in the figure for high magnetic fields. In this case, the ^{0}LH$\downarrow$ state is given by the V_{02} band.

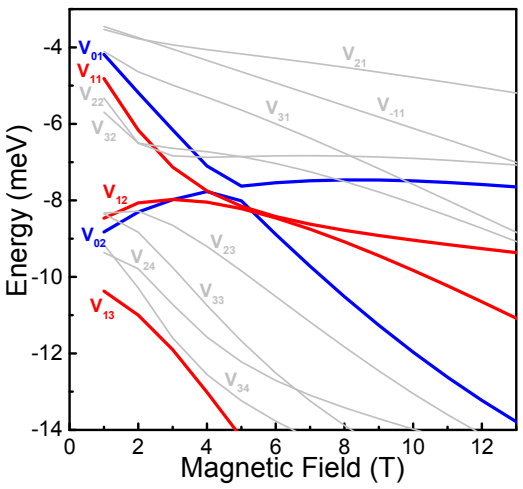

FIG. 5. (Color online) The calculated valence band subband energy levels for the GaAs/AlGaAs multiple quantum well structure. The subbands and their labels have been colored to match their Pidgeon-Brown (PB) manifolds with $p = 0$ being blue and $p = 1$ being red. V_{ij} labels correspond to the jth valence band state for the $p = i$ PB manifold. That is, V_{12} is the valence band state with the second highest energy in the $p = 1$ PB manifold. Highlighted here (from Table I) the ^{0}LH$\downarrow$ state lies in the $p = 0$ manifold (blue), and the ^{0}LH$\uparrow$ states lies within the $p = 1$ manifold (red).

This is in contrast to the states in the $p = 1$ manifold (red). The mixing of these states is shown in Table III. Strong field-dependent mixing is observed for these states. For low magnetic fields, ^{0}LH$\uparrow$ consists mainly of V_{13}, but there is a cross-over so that at high magnetic fields, V_{11} becomes dominated by the ^{0}LH$\uparrow$ component. This immediately explains why the energy difference between the LH spin-up and spin-down lowest LLs is **not** linear, as one might expect. The ^{0}LH$\downarrow$ and the ^{0}LH$\uparrow$ LLs *have significantly different dependences on magnetic field* B_0.

In Fig. 6, we plot the spin-polarization, $(\alpha\uparrow - \alpha\downarrow)/(\alpha\uparrow + \alpha\downarrow)$, where $\alpha\uparrow$ and $\alpha\downarrow$ are the absorptions that produce spin-up/spin-down CB electrons, respectively. Since there is very little CB mixing, the CBs are almost 100% spin pure (typically they are 99% of a fixed spin or better). To calculate the $\alpha\uparrow$ absorption, we calculate the absorption to the CB that is

B_0(T)	Wavefunction Probability(%)			
	V_{02}		V_{01}	
	^{1}HH↓	^{0}LH↓	^{1}HH↓	^{0}LH↓
1	22	78	99	1
2	25	75	98	1
3	26	74	97	3
4	26	74	96	4
4.7	95	5	26	74
5	94	6	26	74
6	93	7	26	74
7	91	9	25	75
8	89	11	25	75
9	86	14	24	76
10	84	16	24	76
11	82	18	23	77
11.8	80	20	23	77
12	79	21	23	77

TABLE II. Wavefunction mixing in valence subbands for $p = 0$ at different magnetic fields (B_0).

B_0(T)	Wavefunction Probability(%)								
	V_{11}			V_{12}			V_{13}		
	^{2}HH↓	^{1}LH↓	^{0}LH↑	^{2}HH↓	^{1}LH↓	^{0}LH↑	^{2}HH↓	^{1}LH↓	^{0}LH↑
1	97	2	1	28	72	0	2	0	98
2	88	4	8	31	69	0	8	0	92
3	75	5	20	32	68	0	19	2	79
4	60	5	35	32	68	0	30	5	65
4.7	52	6	42	32	68	0	36	7	57
5	49	6	45	32	68	0	37	8	54
6	42	6	52	31	68	1	41	13	46
7	37	6	57	31	68	1	42	18	40
8	33	6	61	31	68	1	42	22	35
9	30	7	63	31	68	1	42	27	31
10	28	7	65	30	68	1	41	30	28
11	26	7	67	30	68	2	41	33	26
11.8	25	7	68	30	68	2	40	35	25
12	25	7	68	30	68	2	40	36	24

TABLE III. Wavefunction mixing in valence subbands for $p = 1$ at different magnetic fields (B_0).

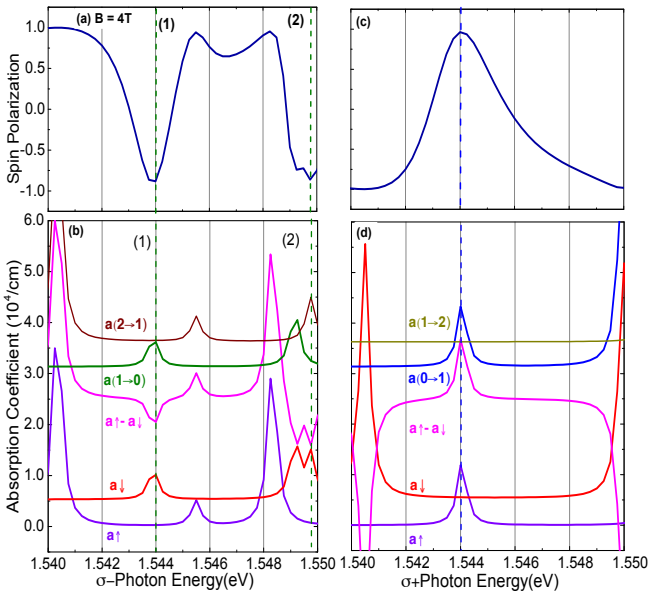

FIG. 6. (Color online) Calculated spin polarization (a) and (c) and manifold-resolved absorption coefficients (b) and (d) for $\sigma+$ and $\sigma-$ photon energies at $B_0 = 4$ T. The colors and cutoffs are chosen for clarity. Note that transitions at $p = 0, 1$, and 2 along with total spin-up $\alpha\uparrow$ (purple), total spin-down $\alpha\downarrow$ (red), and difference $\alpha\uparrow$-$\alpha\downarrow$ (magenta) are included. These results show that the dip (peak) in the σ^- (σ^+) absorption (dashed vertical lines) corresponds to the absorption transitions from the light holes.

spin-up. In Fig. 6 (a), we show the CB-spin polarization for σ^- circular polarization and in (c) we show the CB-spin polarization for σ^+ excitation. In (b) we plot the manifold resolved absorption for σ^- polarization, as well as $\alpha\uparrow$ and $\alpha\downarrow$. For example, we observe that the $\alpha\downarrow$ absorption is dominated at 1.544 eV by the transition from the $1 \rightarrow 0$ PB manifolds. In (d) we do the same for σ^+ polarization. For σ^- polarization, excitation from a LH level will produce spin-down conduction electrons while excitation from a HH level will produce spin-up conduction electrons. The opposite is true for σ^+ polarization. By comparing (a) and (b), we see that the dip in the polarization occurs when there is absorption from the LH levels. Also comparing (c) and (d), the peak in the absorption occurs when one has a transition from a LH level.

To make contact with experiment, we plot the CB spin-down absorption (Fig. 7) for σ^- polarization and the CB spin-up polarization for σ^+ polarization (Fig. 8). *Peaks in these spectra correspond to LH-to-CB transitions in the $n = 0$ LLs.* They can be compared directly to the OPNMR experimental results plotted in Fig. 3. By comparing the figures we notice several features.

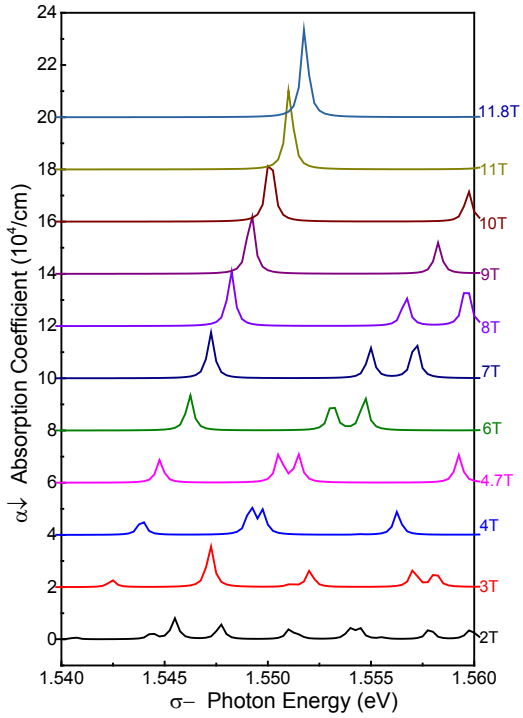

FIG. 7. (Color online) Calculated conduction band spin-down absorption coefficients for $\sigma-$ photon energy at different B_0 values (2 – 11.8 T).

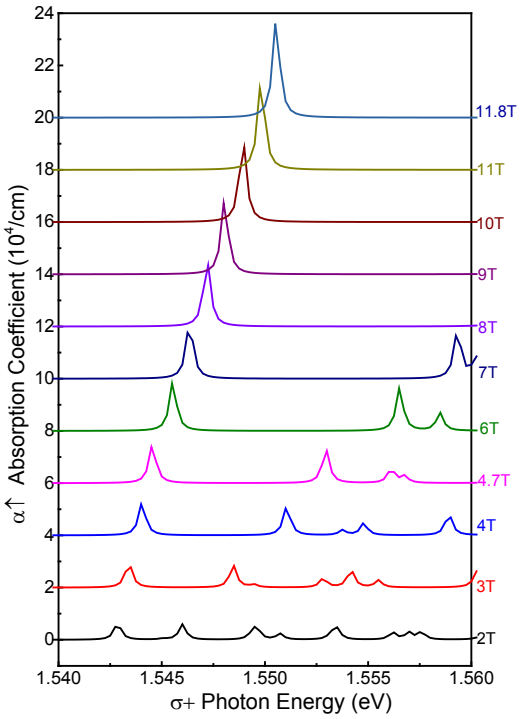

FIG. 8. (Color online) Calculated conduction band spin-up absorption coefficients for $\sigma+$ photon energy at different B_0 values (2 – 11.8 T).

1. The dominant peak for σ^- absorption is at higher photon energy than the dominant peak for σ^+ absorption which is consistent with experiment. Separations between the peaks for the different polarizations at the same magnetic field are also consistent with experiment.

2. The calculated peaks have a greater shift with magnetic field than the experimental shifts. In fact, the experimental peaks (dips) shift by an amount less than $eB_0/2m_e^*c$, which is the shift in the CB $n = 0$ LL. We see from Fig. 5 that part of the reason is that the LH bands initially *increase in energy with magnetic field*, between 0 and 4 T. However, we note that this is still not enough to reproduce the experimental data shown in Fig. 4 in the same region. The most likely cause for this discrepancy is excitonic effects. It is well known that excitonic effects decrease the slope of the transition energy vs. magnetic field plot, especially for the lowest lying Landau levels[23]. Even though the LH bands are well below the valence band maximum, the experimental results indicate that excitonic effects are still important, though difficult to include in calculations. Therefore, most theoretical models of excitons in quantum wells include only the highest lying bands.

   We should also note that other effects not included in the model might lead to the greater calculated shifts compared to those seen experimentally. These include: i) strain at the interfaces (while in principle, the wells and barriers are lattice matched, any source of strain can change the energy levels dramatically, as we have previously calculated[11]. ii) carrier doping in the wells can change the potentials and energy levels. iii) The GaAs substrate can influence the signal as we have previously shown[10].

3. We note that for σ^- polarization, the dominant peak at low fields is the second peak, while at high field it is the first peak. This is related to the VB mixing between V_{11} and V_{13} discussed above, as the nature of the bands changes due to the mixing. Furthermore, if we look at the experimental data for σ^- in Fig. 3, we see that there is indeed a second, weaker feature seen in this cross-over regime between 3 – 5 T (even though it does not change the sign of the polarization). We suspect that this feature is real and is related to this cross-over due to the band mixing.

IV. CONCLUSIONS

In summary, the photon energy dependence of optically-pumped ^{69}Ga and ^{71}Ga NMR signals of an AlGaAs/GaAs multiple quantum well sample was measured

at a series of externally applied magnetic fields (B_0) ranging from 3 T to 11.8 T. The light hole-to-conduction band transition dominates these OPNMR profiles, where the integrated OPNMR signal intensity is plotted with respect to photon energy used for optical pumping. Additionally, the measurements of the transition energy were extended by collection of polarized PLE data at 0 T and 3 T. The PLE measurements are included here in order to establish a zero-field measurement and to show the good agreement between both PLE and OPNMR measurements of similar phenomena. The magnetic field dependence of the dominant peak in the OPNMR profiles is found to be linear for σ^- circularly polarized optical pumping light. In contrast, the energy of the dominant peak in the OPNMR profile obtained with σ^+ irradiation is non-linear at low field but becomes approximately linear at high magnetic fields (B_0= 6 to 12 T). The OPNMR data were validated by repeating a subset of the measurements in a second experimental setup using similar measurement parameters.

Interpretation of the field dependence of the OPNMR photon energy profiles was facilitated by electronic band structure theory. The two opposing helicities of the pumping light excite transitions from different initial states. The strong curvature in the magnetic field dependence of the OPNMR data collected with σ^+ light was explained by the effects of Landau level mixing on the LH↓ subband. Clearly, the proper interpretation of the field dependence of the OPNMR profiles requires simulations of the subband energy levels. In fact, it is only through such simulations that the mixing of valence band Landau levels can be quantified and interpreted, including the swapping of transition probabilities between pairs of Pidgeon-Brown basis states. The simulations permit optical absorption coefficients to be computed and analyzed. The calculations reveal that the dominant transition for σ^- absorption occurs at higher energy than that of σ^+. Hence, the comprehensive understanding of the field dependence of Landau level mixing in the HH and LH states can account for the very different field dependences observed for the dominant transition in the OPNMR profiles obtained with left and right circularly polarized pumping light.

ACKNOWLEDGMENTS

This work was supported by the NSF through Grant No. DMR-1105437, DMR-1206447 (SEH, ELS, MMW, CJS, SKT) and by the National High Magnetic Field Laboratory's User Collaborative Grants Program (UCGP) (SM, PK, APR, CJS, CRB, RMW, SEH, MMW). A portion of this work was performed at the National High Magnetic Field Laboratory, which is supported by National Science Foundation Cooperative Agreement No. DMR-1157490, the State of Florida and the U.S. Department of Energy. CJS also received support from the Air Force Office of Scientific Research under award number FA9550-17-1-0341. The authors would like to acknowledge Dr. Soheyla Eshlaghi in Professor Andreas Wieck's group for synthesizing the quantum well sample studied in this paper.

* hayes@wustl.edu, stanton@phys.ufl.edu

[1] M. Dyakonov and V. Perel, in *Optical Orientation*, Vol. 8 (1984) pp. 15–71.
[2] S. E. Barrett, R. Tycko, L. N. Pfeiffer, and K. W. West, Phys. Rev. Lett. **72**, 1368 (1994).
[3] R. Tycko and J. A. Reimer, J. Phys. Chem. **3654**, 13240 (1996).
[4] P. L. Kuhns, A. Kleinhammes, T. Schmiedel, W. G. Moulton, P. Chabrier, S. Sloan, E. Hughes, and C. R. Bowers, Physical Review B **55**, 7824 (1997).
[5] A. Patel, O. Pasquet, J. Bharatam, E. Hughes, and C. R. Bowers, Physical Review B **60**, 5105 (1999).
[6] S. E. Hayes, S. Mui, and K. Ramaswamy, The Journal of Chemical Physics **128**, 052203 (2008).
[7] D. D. Wheeler, M. M. Willmering, E. L. Sesti, X. Pan, D. Saha, C. J. Stanton, and S. E. Hayes, Journal of Magnetic Resonance **273**, 19 (2016).
[8] M. M. Willmering, Z. L. Ma, M. A. Jenkins, J. F. Conley, and S. E. Hayes, Journal of the American Chemical Society **139**, 3930 (2017).
[9] K. Ramaswamy, S. Mui, S. a. Crooker, X. Pan, G. D. Sanders, C. J. Stanton, and S. E. Hayes, Physical Review B - Condensed Matter and Materials Physics **82**, 1 (2010).
[10] E. L. Sesti, D. Saha, D. D. Wheeler, G. D. Sanders, S. E. Hayes, and C. J. Stanton, Physical Review B **90**, 125301 (2014).
[11] R. M. Wood, D. Saha, L. a. McCarthy, J. T. Tokarski, G. D. Sanders, P. L. Kuhns, S. a. McGill, a. P. Reyes, J. L. Reno, C. J. Stanton, and C. R. Bowers, Physical Review B **90**, 155317 (2014).
[12] E. L. Sesti, W. Worthoff, D. D. Wheeler, D. Suter, and S. E. Hayes, Journal of Magnetic Resonance **246**, 130 (2014).
[13] R. Planel, Solid-State Electronics **21**, 1437 (1978).
[14] R. Tycko, S. E. Barrett, G. Dabbagh, L. N. Pfeiffer, and K. W. West, Science **268**, 1460 (1995).
[15] $\gamma_n/2\pi$ = 10.248 MHz/T for ^{69}Ga and 13.021 MHz/T for ^{71}Ga.
[16] M. Kubisa, L. Bryja, K. Ryczko, J. Misiewicz, C. Bardot, M. Potemski, G. Ortner, M. Bayer, a. Forchel, and C. Sø rensen, Physical Review B **67**, 035305 (2003).
[17] D. Broido and L. Sham, Physical Review B **31**, 888 (1985).
[18] E. S.-R. Yang, D. A. Broido, and L. J. Sham, Physical Review B **32**, 6630 (1985).
[19] K. Ryczko, M. Kubisa, L. Bryja, J. Misiewicz, R. Stpniewski, M. Byszewski, and M. Potemski, Physica B: Condensed Matter **346-347**, 451 (2004).

[20] F. Ancilotto, a. Fasolino, and J. Maan, Superlattices and Microstructures **3**, 187 (1987).
[21] R. Winkler, "Spin-orbit coupling effects in two-dimensional electron and hole systems," (Springer Berlin Heidelberg, 2003) p. 53.
[22] N. Kamaraju, W. Pan, U. Ekenberg, D. M. Gvozdić, S. Boubanga-Tombet, P. C. Upadhya, J. Reno, A. J. Taylor, and R. P. Prasankumar, Applied Physics Letters **106**, 031902 (2015).
[23] J. G. Mavroides, in *Optical Properties of Solids*, edited by F. Abelès (North-Holland Pub. Co., 1972) Chap. 7.